Acta Cryst E
CRYSTALLOGRAPHIC COMMUNICATIONS

ISSN 2056-9890

Crystal structure and Hirshfeld surface analysis of 2-bromoethylammonium bromide – a possible side product upon synthesis of hybrid perovskites

Oleksandr A. Semenikhin,[a]* Sergiu Shova,[b] Irina A. Golenya,[a] Dina D. Naumova[a] and Il'ya A. Gural'skiy[a]

[a]Department of Chemistry, Taras Shevchenko National University of Kyiv, Volodymyrska St. 64, Kyiv 01601, Ukraine, and [b]Department of Inorganic Polymers, Petru Poni Institute of Macromolecular Chemistry, Aleea Grigore Ghica Voda 41-A, Iasi 700487, Romania. *Correspondence e-mail: alex.semenikhin@knu.ua

Received 24 May 2024
Accepted 11 June 2024

Edited by M. Weil, Vienna University of Technology, Austria

Keywords: crystal structure; Hirshfeld surface analysis; 2-bromoethylamine hydrobromide; hybrid perovskite.

CCDC reference: 2362029

Supporting information: this article has supporting information at journals.iucr.org/e

This study presents the synthesis, characterization and Hirshfeld surface analysis of a small organic ammonium salt, $C_2H_7BrN^+\cdot Br^-$. Small cations like the one in the title compound are considered promising components of hybrid perovskites, crucial for optoelectronic and photovoltaic applications. While the incorporation of this organic cation into various hybrid perovskite structures has been explored, its halide salt counterpart remains largely uninvestigated. The obtained structural results are valuable for the synthesis and phase analysis of hybrid perovskites. The title compound crystallizes in the solvent-free form in the centrosymmetric monoclinic space group $P2_1/c$, featuring one organic cation and one bromide anion in its asymmetric unit, with a torsion angle of −64.8 (2)° between the ammonium group and the bromine substituent, positioned in a *gauche* conformation. The crystal packing is predominantly governed by Br⋯H interactions, which constitute 62.6% of the overall close atom contacts.

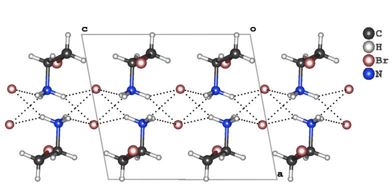

1. Chemical context

Hybrid perovskites have emerged as a class of highly promising compounds for a wide array of applications in optoelectronics and photovoltaics due to their semiconducting properties. Among these, perovskites with a tri-periodic arrangement have garnered significant attention owing to their optimal bandgap width (Dey *et al.*, 2021; Liu *et al.*, 2021; Hassan *et al.*, 2021; Yoo *et al.*, 2021). Notably, the aziridinium cation (AzrH) has recently been shown to support such perovskite structures. In the form (AzrH)BX_3 (B = Pb, Sn; X = Br, I; Petrosova *et al.*, 2022; Kucheriv *et al.*, 2023), these perovskites display promising physical properties (Mączka *et al.*, 2023; Stefańska *et al.*, 2022), and nanomaterials based on them offer potential for various applications (Semenikhin *et al.*, 2023; Bodnarchuk *et al.*, 2024).

The high reactivity of aziridine poses a synthetic challenge as it can undergo ring-opening in acidic environments, leading to the formation of perovskites with low periodicity such as $(X(CH_2)_2NH_3)_{2n}(BX)_{4n}$ (B = Pb, Sn; X = Br, I; Skorokhod *et al.*, 2023; Song *et al.*, 2022; Sourisseau *et al.*, 2007; Lemmerer & Billing, 2010) and 2-bromoethylammonium bromide as a side product. However, these perovskite materials also often manifest physical properties that are as well worth exploring.

In this study, we present the crystal structure analysis and Hirshfeld surface analysis of an organic–inorganic hybrid salt, $C_2H_7BrN^+Br^-$. While this organic cation has previously been incorporated into various hybrid perovskite structures, its halide salt counterpart remains unexplored, representing a significant gap in analysis of these materials. Knowledge of its structure is also important for the phase analysis of studied aziridinium-based materials.

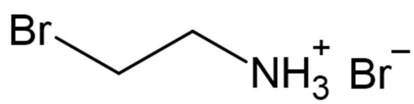

2. Structural commentary

The title compound crystallizes in a solvent-free form and consists of one organic cation and one bromide anion in the asymmetric unit (Fig. 1). The backbone of the cation, N1, C2, C1, Br1, has a torsion angle of −64.8 (2)°, with the atoms positioned in a *gauche* conformation. The N1—C2 and C1—C2 bonds have lengths of 1.480 (3) and 1.513 (4) Å, respectively. These values are typical for protonated alkylamines and consistent with previous reports (Ishida, 2000). The C1—Br1 length is 1.953 (3) Å, which is also a typical value for C—*X* length in alkyl halides (Allen *et al.*, 1987).

3. Intermolecular features

Fig. 2 shows a view of the structure along the *b* axis, which illustrates the intermolecular organization through N—H⋯Br hydrogen bonds, revealing that each bromide anion is the acceptor of four contacts with NH_3^+ groups. Corresponding numerical data are given in Table 1. Our analysis uncovered different patterns of hydrogen-bonding interactions. Specifically, N1—H1*A*⋯Br2 and N1—H1*B*⋯Br2^{i} [symmetry code: (i) $-x+1, -y+1, -z+1$] interactions demonstrate typical classical behavior, with angles of 156.1° and 156.2°, and *D*⋯*A* distances of 3.3010 (19) Å and 3.381 (2) Å, respectively. In contrast, N1—H1*C*⋯Br2^{ii} and N1—H1*C*⋯Br2^{iii} [symmetry codes: (ii) $x, -y+\frac{1}{2}, z+\frac{1}{2}$; (iii) $-x+1, y+\frac{1}{2}, -z+\frac{3}{2}$] contacts exhibit weaker interactions, with longer *D*⋯*A* distances of 3.3904 (19) and 3.4292 (18) Å, and angles of 125.1° and 140.3°. Fig. 3 shows that the arrangement of cations and anions leads to the formation of double layers.

Table 1
Hydrogen-bond geometry (Å, °).

D—H⋯*A*	*D*—H	H⋯*A*	*D*⋯*A*	*D*—H⋯*A*
N1—H1*A*⋯Br2	0.85	2.51	3.3010 (19)	156
N1—H1*B*⋯Br2^{i}	0.85	2.59	3.381 (2)	156
N1—H1*C*⋯Br2^{ii}	0.85	2.83	3.3904 (19)	125
N1—H1*C*⋯Br2^{iii}	0.85	2.73	3.4292 (18)	140

Symmetry codes: (i) $-x+1, -y+1, -z+1$; (ii) $x, -y+\frac{1}{2}, z+\frac{1}{2}$; (iii) $-x+1, y+\frac{1}{2}, -z+\frac{3}{2}$.

4. Hirshfeld analysis

The intermolecular interactions in 2-bromoethylammonium bromide were analyzed using Hirshfeld surface calculations, employing *CrystalExplorer* (Spackman *et al.*, 2021). Results are plotted over the d_{norm} range between −0.4077 and +1.2052 a.u. (Spackman & Jayatilaka, 2009). A three-dimensional model of the Hirshfeld surface (Fig. 4) highlights strong

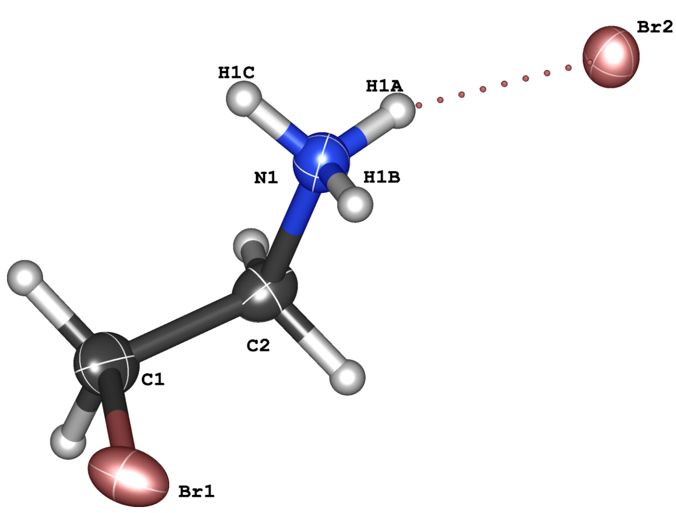

Figure 1
The asymmetric unit of 2-bromoethylammonium bromide with displacement ellipsoids drawn at the 50% probability level. The dotted line represents the hydrogen bond between the cation and anion.

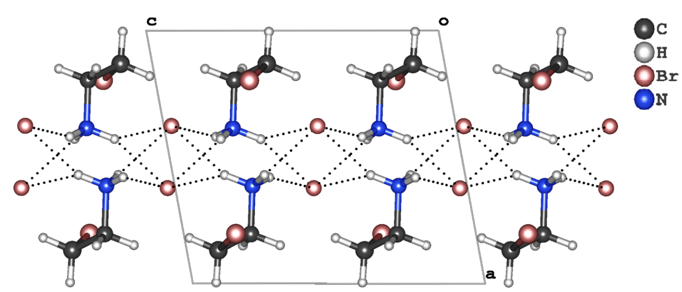

Figure 2
Projection of the crystal structure along the *b* axis, showing the hydrogen-bonding interactions with the anion being an acceptor of four N—H⋯Br hydrogen bonds.

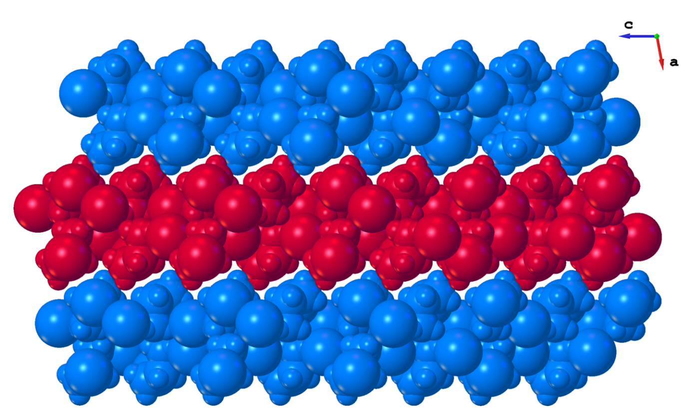

Figure 3
Space-filling model of the title compound showing the organization into double layers extending parallel to (100).

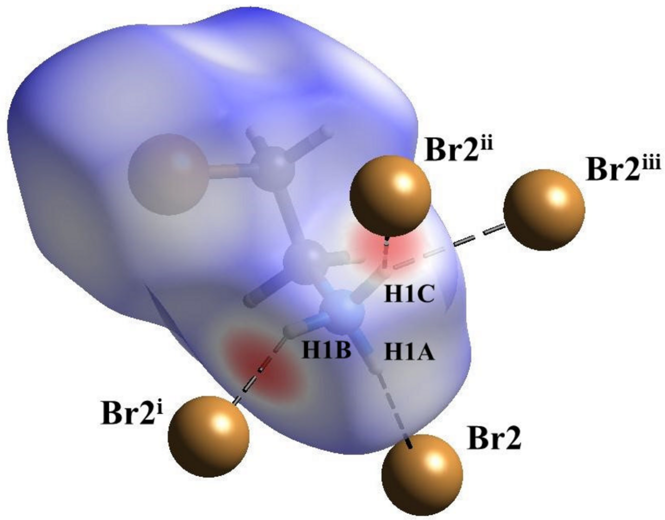

Figure 4
Three-dimensional model of the Hirshfeld surface for 2-bromoethylammonium bromide mapped over d_{norm}, representing strong intermolecular interactions. [Symmetry codes: (i) $-x + 1, -y + 1, -z + 1$; (ii) $x, -y + \frac{1}{2}, z + \frac{1}{2}$; (iii) $-x + 1, y + \frac{1}{2}, -z + \frac{3}{2}$.]

Br···H/H···Br contacts, exhibiting a cation volume of 103.45 Å, a surface area of 119.7 Å, a globularity of 0.890, and an asphericity of 0.059. Additionally, two-dimensional fingerprint plots were generated, illustrating all specific intermolecular contacts (McKinnon *et al.*, 2007). Fig. 5 shows Br···H/H···Br, Br···Br interactions, and all interactions present in the structure with meaningful intermolecular contacts. In the crystal packing, Br···H interactions predominate, constituting 62.6% of the overall close atom contacts, while Br···Br interactions contribute with 2.6%, and H···H contacts account for 34.8%, indicating no additional interactions involving the heteroatoms.

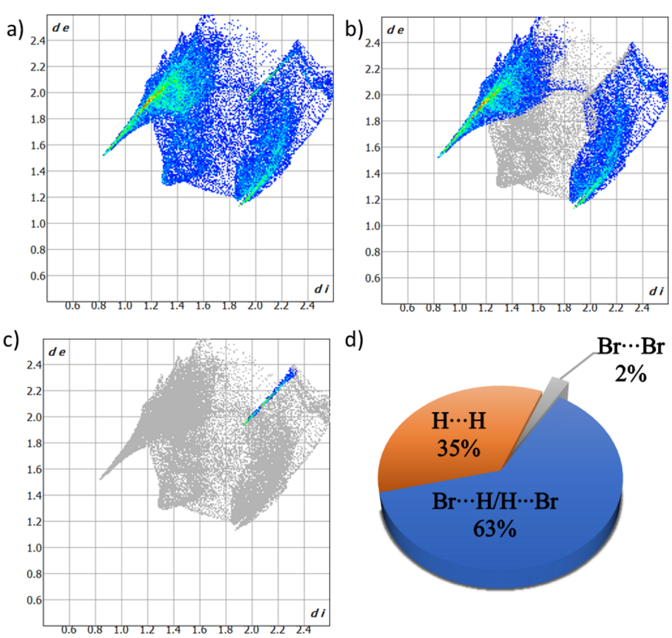

Figure 5
Two-dimensional fingerprint plots of 2-bromoethylammonium bromide showing (*a*) all interactions, (*b*) Br···H/H···Br and (*c*) Br···Br interactions (d_i and d_e are the closest internal and external distances in Å on the Hirshfeld surface) and (*d*) their percentage contributions.

Table 2
Experimental details.

Crystal data	
Chemical formula	$C_2H_7BrN^+\cdot Br^-$
M_r	204.91
Crystal system, space group	Monoclinic, $P2_1/c$
Temperature (K)	200
a, *b*, *c* (Å)	7.8966 (4), 8.3394 (4), 9.0089 (4)
β (°)	100.546 (5)
V (Å^3)	583.24 (5)
Z	4
Radiation type	Mo *K*α
μ (mm^{-1})	13.75
Crystal size (mm)	0.15 × 0.05 × 0.02
Data collection	
Diffractometer	XtaLAB Synergy, Dualflex, HyPix
Absorption correction	Multi-scan (*CrysAlis PRO*; Rigaku OD, 2024)
T_{min}, T_{max}	0.451, 1.000
No. of measured, independent and observed [$I > 2\sigma(I)$] reflections	4504, 1453, 1242
R_{int}	0.024
$(\sin \theta/\lambda)_{max}$ (Å^{-1})	0.709
Refinement	
$R[F^2 > 2\sigma(F^2)]$, $wR(F^2)$, S	0.024, 0.054, 1.04
No. of reflections	1453
No. of parameters	49
H-atom treatment	H atoms treated by a mixture of independent and constrained refinement
$\Delta\rho_{max}$, $\Delta\rho_{min}$ (e Å^{-3})	0.56, −0.47

Computer programs: *CrysAlis PRO* (Rigaku OD, 2024), *SHELXT* (Sheldrick, 2015*a*), *SHELXL* (Sheldrick, 2015*b*) and *OLEX2* (Dolomanov *et al.*, 2009).

5. Synthesis and crystallization

All chemicals were purchased from Enamine Ltd (Kyiv, Ukraine) and used without any further purification. Aziridine (258.4 µl, 5 mmol) was added dropwise under stirring to 2 ml of conc. HBr, gradually heated to 353 K until water evaporation occurred and colorless crystals formed. The obtained crystals were left under Paratone(R) oil until the X-ray measurement.

6. Refinement

Crystal data, data collection and structure refinement details are summarized in Table 2. Hydrogen atoms were placed at calculated positions with $U_{iso}(H) = 1.2U_{eq}(C,N)$. Hydrogens atom of CH_2 group were included in idealized positions (C—H = 0.99 Å).

Funding information

Funding for this research was provided by the EURIZON project, which is funded by the European Union (grant No. 871072).

References

Allen, F. H., Kennard, O., Watson, D. G., Brammer, L., Orpen, A. G. & Tailor, R. (1987). *J. Chem. Soc. Perkin Trans. 2*, pp. 1–19.

Bodnarchuk, M. I., Feld, L. G., Zhu, C., Boehme, S. C., Bertolotti, F., Avaro, J., Aebli, M., Mir, S. H., Masciocchi, N., Erni, R., Chakraborty, S., Guagliardi, A., Rainò, G. & Kovalenko, M. V. (2024). *ACS Nano*, **18**, 5684–5697.

Dey, A., Ye, J., De, A., Debroye, E., Ha, S. K., Bladt, E., Kshirsagar, A. S., Wang, Z., Yin, J., Wang, Y., Quan, L. N., Yan, F., Gao, M., Li, X., Shamsi, J., Debnath, T., Cao, M., Scheel, M. A., Kumar, S., Steele, J. A., Gerhard, M., Chouhan, L., Xu, K., Wu, X. G., Li, Y., Zhang, Y., Dutta, A., Han, C., Vincon, I., Rogach, A. L., Nag, A., Samanta, A., Korgel, B. A., Shih, C. J., Gamelin, D. R., Son, D. H., Zeng, H., Zhong, H., Sun, H., Demir, H. V., Scheblykin, I. G., Mora-Seró, I., Stolarczyk, J. K., Zhang, J. Z., Feldmann, J., Hofkens, J., Luther, J. M., Pérez-Prieto, J., Li, L., Manna, L., Bodnarchuk, M. I., Kovalenko, M. V., Roeffaers, M. B. J., Pradhan, N., Mohammed, O. F., Bakr, O. M., Yang, P., Müller-Buschbaum, P., Kamat, P. V., Bao, Q., Zhang, Q., Krahne, R., Galian, R. E., Stranks, S. D., Bals, S., Biju, V., Tisdale, W. A., Yan, Y., Hoye, R. L. Z. & Polavarapu, L. (2021). *ACS Nano*, **15**, 10775–10981.

Dolomanov, O. V., Bourhis, L. J., Gildea, R. J., Howard, J. A. K. & Puschmann, H. (2009). *J. Appl. Cryst.* **42**, 339–341.

Hassan, Y., Park, J. H., Crawford, M. L., Sadhanala, A., Lee, J., Sadighian, J. C., Mosconi, E., Shivanna, R., Radicchi, E., Jeong, M., Yang, C., Choi, H., Park, S. H., Song, M. H., De Angelis, F., Wong, C. Y., Friend, R. H., Lee, B. R. & Snaith, H. J. (2021). *Nature*, **591**, 72–77.

Ishida, H. (2000). *Z. Naturforsch. Teil A*, **55**, 769–771.

Kucheriv, O. I., Sirenko, V. Y., Petrosova, H. R., Pavlenko, V. A., Shova, S. & Gural'skiy, I. A. (2023). *Inorg. Chem. Front.* **10**, 6953–6963.

Lemmerer, A. & Billing, D. G. (2010). *CrystEngComm*, **12**, 1290–1301.

Liu, X.-K., Xu, W., Bai, S., Jin, Y., Wang, J., Friend, R. H. & Gao, F. (2021). *Nat. Mater.* **20**, 10–21.

Mączka, M., Ptak, M., Gągor, A., Zaręba, J. K., Liang, X., Balčiūnas, S., Semenikhin, O. A., Kucheriv, O. I., Gural'skiy, I. A., Shova, S., Walsh, A., Banys, J. & Šimėnas, M. (2023). *Chem. Mater.* **35**, 9725–9738.

McKinnon, J. J., Jayatilaka, D. & Spackman, M. A. (2007). *Chem. Commun.* pp. 3814–3816.

Petrosova, H. R., Kucheriv, O. I., Shova, S. & Gural'skiy, I. A. (2022). *Chem. Commun.* **58**, 5745–5748.

Rigaku OD (2024). *CrysAlis PRO*. Rigaku Oxford Diffraction, Yarnton, England.

Semenikhin, O. A., Kucheriv, O. I., Sacarescu, L., Shova, S. & Gural'skiy, I. A. (2023). *Chem. Commun.* **59**, 3566–3569.

Sheldrick, G. M. (2015*a*). *Acta Cryst.* A**71**, 3–8.

Sheldrick, G. M. (2015*b*). *Acta Cryst.* C**71**, 3–8.

Skorokhod, A., Quarti, C., Abhervé, A., Allain, M., Even, J., Katan, C. & Mercier, N. (2023). *Chem. Mater.* **35**, 2873–2883.

Song, Z., Yu, B., Wei, J., Li, C., Liu, G. & Dang, Y. (2022). *Inorg. Chem.* **61**, 6943–6952.

Sourisseau, S., Louvain, N., Bi, W., Mercier, N., Rondeau, D., Buzaré, J.-Y. & Legein, C. (2007). *Inorg. Chem.* **46**, 6148–6154.

Spackman, M. A. & Jayatilaka, D. (2009). *CrystEngComm*, **11**, 19–32.

Spackman, P. R., Turner, M. J., McKinnon, J. J., Wolff, S. K., Grimwood, D. J., Jayatilaka, D. & Spackman, M. A. (2021). *J. Appl. Cryst.* **54**, 1006–1011.

Stefańska, D., Ptak, M. & Mączka, M. (2022). *Molecules*, **27**, 7949–7960.

Yoo, J. J., Seo, G., Chua, M. R., Park, T. G., Lu, Y., Rotermund, F., Kim, Y.-K., Moon, C. S., Jeon, N. J., Correa-Baena, J.-P., Bulović, V., Shin, S. S., Bawendi, M. G. & Seo, J. (2021). *Nature*, **590**, 587–593.

supporting information

Acta Cryst. (2024). E**80**, 738-741 [https://doi.org/10.1107/S2056989024005619]

Crystal structure and Hirshfeld surface analysis of 2-bromoethylammonium bromide – a possible side product upon synthesis of hybrid perovskites

Oleksandr A. Semenikhin, Sergiu Shova, Irina A. Golenya, Dina D. Naumova and Il'ya A. Gural'skiy

Computing details

2-Bromoethylammonium bromide

Crystal data

$C_2H_7BrN^+\cdot Br^-$
M_r = 204.91
Monoclinic, $P2_1/c$
a = 7.8966 (4) Å
b = 8.3394 (4) Å
c = 9.0089 (4) Å
β = 100.546 (5)°
V = 583.24 (5) Å^3
Z = 4
$F(000)$ = 384
D_x = 2.334 Mg m^{-3}
Mo $K\alpha$ radiation, λ = 0.71073 Å
Cell parameters from 2526 reflections
θ = 2.6–30.0°
μ = 13.75 mm^{-1}
T = 200 K
Plate, clear intense colourless
0.15 × 0.05 × 0.02 mm

Data collection

XtaLAB Synergy, Dualflex, HyPix diffractometer
Radiation source: micro-focus sealed X-ray tube, PhotonJet (Mo) X-ray Source
Mirror monochromator
Detector resolution: 10.0000 pixels mm^{-1}
ω scans
Absorption correction: multi-scan (CrysAlisPro; Rigaku OD, 2024)
T_{min} = 0.451, T_{max} = 1.000
4504 measured reflections
1453 independent reflections
1242 reflections with $I > 2\sigma(I)$
R_{int} = 0.024
θ_{max} = 30.3°, θ_{min} = 2.6°
$h = -10 \rightarrow 10$
$k = -10 \rightarrow 11$
$l = -12 \rightarrow 12$

Refinement

Refinement on F^2
Least-squares matrix: full
$R[F^2 > 2\sigma(F^2)]$ = 0.024
$wR(F^2)$ = 0.054
S = 1.04
1453 reflections
49 parameters
0 restraints
Primary atom site location: dual
Hydrogen site location: inferred from neighbouring sites
H atoms treated by a mixture of independent and constrained refinement
$w = 1/[\sigma^2(F_o^2) + (0.028P)^2]$ where $P = (F_o^2 + 2F_c^2)/3$
$(\Delta/\sigma)_{max}$ = 0.001
$\Delta\rho_{max}$ = 0.56 e Å^{-3}
$\Delta\rho_{min}$ = −0.47 e Å^{-3}
Extinction correction: SHELXL (Sheldrick, 2015b), $Fc^*=kFc[1+0.001xFc^2\lambda^3/\sin(2\theta)]^{-1/4}$
Extinction coefficient: 0.0055 (7)

Special details

Geometry. All esds (except the esd in the dihedral angle between two l.s. planes) are estimated using the full covariance matrix. The cell esds are taken into account individually in the estimation of esds in distances, angles and torsion angles; correlations between esds in cell parameters are only used when they are defined by crystal symmetry. An approximate (isotropic) treatment of cell esds is used for estimating esds involving l.s. planes.

Fractional atomic coordinates and isotropic or equivalent isotropic displacement parameters (Å²)

	x	y	z	U_{iso}*/U_{eq}
Br2	0.62288 (3)	0.21658 (3)	0.52611 (2)	0.02586 (10)
Br1	0.80287 (4)	0.89002 (3)	0.82138 (3)	0.03709 (11)
N1	0.6130 (3)	0.5414 (2)	0.7338 (2)	0.0252 (4)
H1A	0.5825 (5)	0.4579 (15)	0.6819 (15)	0.030*
H1B	0.5747 (6)	0.6239 (14)	0.6835 (16)	0.030*
H1C	0.5728 (7)	0.5380 (17)	0.8149 (12)	0.030*
C2	0.8034 (3)	0.5490 (3)	0.7706 (3)	0.0265 (5)
H2A	0.848456	0.575438	0.678011	0.032*
H2B	0.848904	0.442408	0.806124	0.032*
C1	0.8670 (4)	0.6727 (3)	0.8908 (3)	0.0333 (6)
H1D	0.993935	0.665423	0.918954	0.040*
H1E	0.817760	0.649328	0.981906	0.040*

Atomic displacement parameters (Å²)

	U^{11}	U^{22}	U^{33}	U^{12}	U^{13}	U^{23}
Br2	0.03128 (17)	0.02218 (16)	0.02435 (15)	0.00045 (10)	0.00574 (11)	−0.00179 (9)
Br1	0.02685 (18)	0.03231 (18)	0.0526 (2)	−0.00574 (11)	0.00868 (13)	−0.00512 (11)
N1	0.0289 (12)	0.0227 (10)	0.0238 (10)	0.0008 (9)	0.0048 (9)	0.0001 (8)
C2	0.0235 (14)	0.0286 (13)	0.0286 (12)	0.0067 (11)	0.0076 (10)	0.0059 (10)
C1	0.0256 (15)	0.0420 (15)	0.0294 (13)	−0.0019 (13)	−0.0023 (11)	0.0071 (11)

Geometric parameters (Å, º)

Br1—C1	1.953 (3)	C2—H2A	0.9900
N1—H1A	0.849 (12)	C2—H2B	0.9900
N1—H1B	0.849 (12)	C2—C1	1.513 (4)
N1—H1C	0.849 (12)	C1—H1D	0.9900
N1—C2	1.480 (3)	C1—H1E	0.9900
H1A—N1—H1B	109.5	H2A—C2—H2B	107.9
H1A—N1—H1C	109.5	C1—C2—H2A	109.1
H1B—N1—H1C	109.5	C1—C2—H2B	109.1
C2—N1—H1A	109.5	Br1—C1—H1D	109.3
C2—N1—H1B	109.5	Br1—C1—H1E	109.3
C2—N1—H1C	109.5	C2—C1—Br1	111.77 (17)
N1—C2—H2A	109.1	C2—C1—H1D	109.3
N1—C2—H2B	109.1	C2—C1—H1E	109.3
N1—C2—C1	112.4 (2)	H1D—C1—H1E	107.9

N1—C2—C1—Br1	−64.8 (2)

Hydrogen-bond geometry (Å, º)

D—H···*A*	*D*—H	H···*A*	*D*···*A*	*D*—H···*A*
N1—H1*A*···Br2	0.85	2.51	3.3010 (19)	156
N1—H1*B*···Br2^{i}	0.85	2.59	3.381 (2)	156
N1—H1*C*···Br2^{ii}	0.85	2.83	3.3904 (19)	125
N1—H1*C*···Br2^{iii}	0.85	2.73	3.4292 (18)	140

Symmetry codes: (i) −*x*+1, −*y*+1, −*z*+1; (ii) *x*, −*y*+1/2, *z*+1/2; (iii) −*x*+1, *y*+1/2, −*z*+3/2.